



Targeting EGFR tyrosine kinase: Synthesis, *in vitro* antitumor evaluation, and molecular modeling studies of benzothiazole-based derivatives

Amal M. Mokhtar^a, Shahenda M. El-Messery^b, Mariam A. Ghaly^{a,*}, Ghada S. Hassan^a

^a Department of Medicinal Chemistry, Faculty of Pharmacy, Mansoura University, Mansoura 35516, Egypt

^b Department of Pharmaceutical Organic Chemistry, Faculty of Pharmacy, Mansoura University, Mansoura 35516, Egypt

ARTICLE INFO

Keywords:

Benzothiazole
Synthesis
Antitumor
EGFR
Molecular modeling

ABSTRACT

New benzothiazole-based derivatives were synthesized in the present work with the aim of evaluating their antitumor activity. They were *in vitro* tested against hepatocellular carcinoma (HepG2), colorectal carcinoma (HCT-116), mammary gland cancer (MCF-7), prostate cancer (PC-3), and epithelioid carcinoma (HeLa). The results of the *in vitro* antitumor evaluation revealed that the most active compounds were **39**, **40**, **51**, **56**, and **61** exhibiting IC₅₀ values comparable to the reference drug lapatinib. The most active compounds were further subjected to EGFR inhibitory activity assay to rationalize their potency mode. Notably, the most active antitumor compounds **39** and **40** represented the most potent inhibitors to EGFR with IC₅₀ values of 24.58 and 30.42 nM respectively in comparison with 17.38 nM for lapatinib as a standard drug. Molecular modeling studies were also conducted for the synthesized compounds, including docking into EGFR active site and surface mapping. Results proved the superior binding of the hydrazone derivatives **39** and **40** with EGFR suggesting them as good candidates for targeted antitumor therapy through EGFR kinase inhibition.

1. Introduction

Cancer is an outbreak disease which causes mortality around the world. It is characterized by uncontrolled division and abnormal proliferation of body cells [1]. For years, scientists made many valuable efforts in order to limit the spread of this disease through many strategies. One of the non-traditional strategies is concerned with epidermal growth factor receptor (EGFR).

EGFR is a transmembrane protein that belongs to tyrosine kinase family [2]. It plays a significant role in cell transduction or communication signaling within the cell through phosphorylation (transfer of phosphate group from ATP to the substrate) of tyrosine residues in protein domain. Upregulation or mutation of EGFR results in abnormal cell growth which may lead to appearance of various types of solid malignancies e.g., colon, lung, and cervical cancers, so interruption of EGFR communicating signals can be a suitable choice for decreasing tumors expressed by its misregulation [3]. In contrast to conventional cancer therapies that attack both normal cells and cancer cells resulting in a wide spectrum of side effects which increase patients' suffering, targeted drugs like EGFR tyrosine kinase inhibitors selectively attack cancerous cells rather than normal ones providing a good safety profile, less body damage and more patients' comfortability [4]. Canertinib, erlotinib, and lapatinib are examples of clinically useful EGFR

inhibitors to treat lung and breast cancers [4–6]. They all belong to the class of 4-anilinoquinazolines. Their quinazoline nitrogens mimic the adenine of ATP in binding into the kinase active site, providing hydrogen bonding interactions. In addition, the aniline part is housed in the hydrophobic pocket (Fig. 1).

Benzothiazole is a hetero bicyclic system that has a distinct pharmacological profile including antitumor activity. Many researchers reported the superior EGFR inhibitory activity of substituted benzothiazoles [7–9], some of them displaying more potent antitumor activity than erlotinib as a reference drug [8].

Guided by the above considerations, the work presented herein reports the synthesis of benzothiazole-based derivatives equipped with substituted piperazinoacetamides (9–14), aminothiazolidin-4-ones (23–29), acid hydrazones (35–41), substituted acid hydrazides (44, 45, 50–53, 60 and 61), and triazole-3-thiols (54–57) in which the benzothiazole scaffold was designed as a bioistere to the quinazoline ring system, capable of providing similar competition at the ATP binding site of EGFR. The designed target compounds were subjected to *in vitro* antitumor testing against five cell lines; hepatocellular carcinoma (HepG2), colorectal carcinoma (HCT-116), mammary gland cancer (MCF-7), prostate cancer (PC-3), and epithelioid carcinoma (HeLa), in addition to assessing the EGFR kinase inhibitory activity of the most active antitumor compounds. Molecular modeling studies were also

* Corresponding author.

E-mail address: mariamaghaly@mans.edu.eg (M.A. Ghaly).

<https://doi.org/10.1016/j.bioorg.2020.104259>

Received 3 April 2020; Received in revised form 29 August 2020; Accepted 31 August 2020

Available online 02 September 2020

0045-2068/ © 2020 Elsevier Inc. All rights reserved.

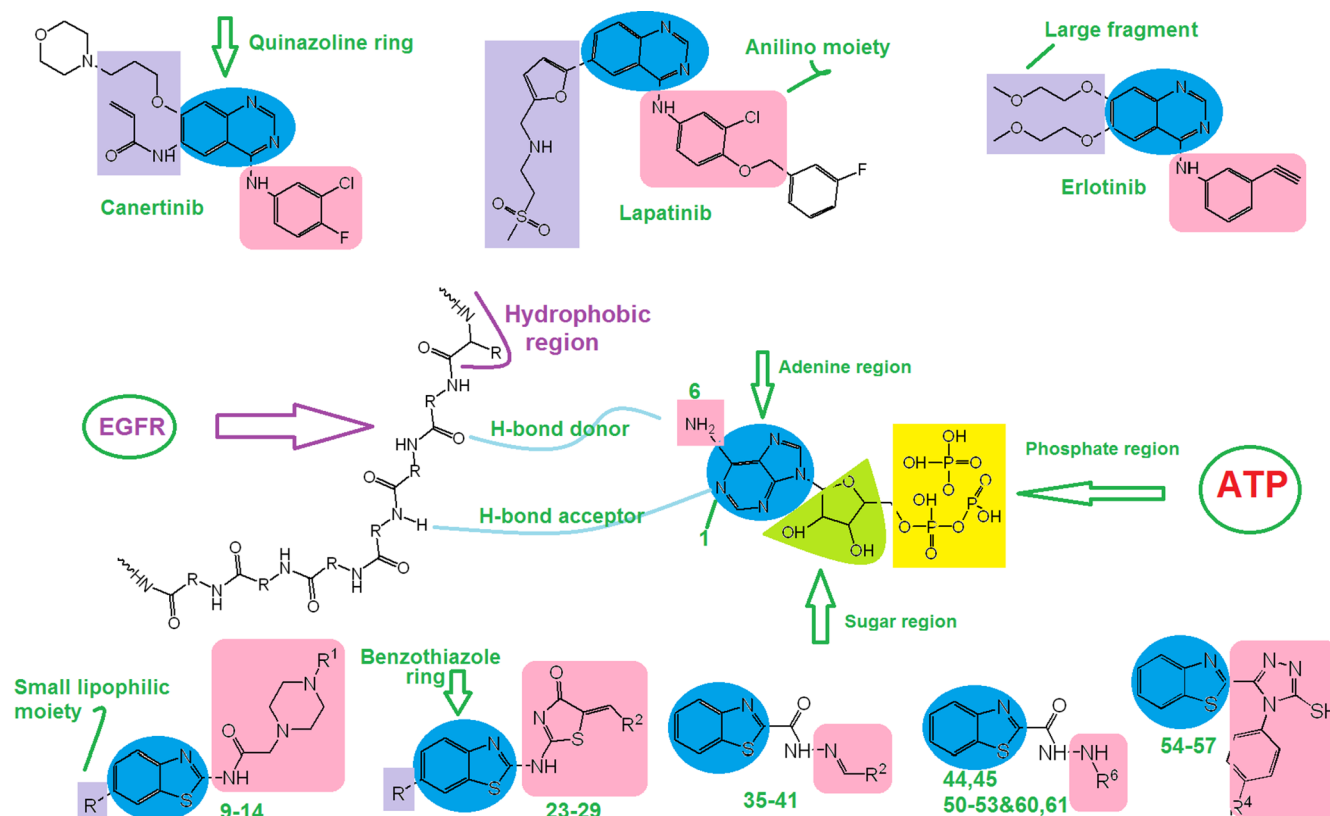


Fig. 1. Clinically approved EFGR inhibitors and the designed target compounds.

performed to rationalize and describe the binding mode of the most active compounds into EGFR kinase active site.

2. Results and discussion

2.1. Chemistry

Syntheses of the designed target compounds were carried out as depicted in Schemes 1–3. In Scheme 1, 2-aminobenzothiazole (1 or 2) was allowed to react with chloroacetyl chloride in chloroform in the presence of triethylamine to afford the corresponding chloroacetamide derivatives 4 and 5. Nucleophilic displacement of the chlorine atom of the latter compounds with different substituted piperazine derivatives (6–8) was achieved in DMF containing anhydrous potassium carbonate yielding the corresponding amino compounds (9–14). The appearance of the piperazine protons as two sets of signals, each integrating for four protons at δ 2.53–2.80 and δ 2.66–3.26 ppm at the expected regions in their ^1H NMR spectra proved the success of the substitution reaction. In addition, reacting 2-chloro-*N*-(6-methylbenzo[*d*]thiazol-2-yl)acetamide (5) with ammonium thiocyanate in boiling ethanol afforded the corresponding 2-aminothiazol-4(5*H*)-one (15). The latter constructed thiazol-4-one was condensed with a variety of aromatic and heteroaromatic aldehydes (16–22) in alcoholic NaOH through Knoevenagel condensation reaction to furnish the corresponding 5-arylidene-thiazol-4(5*H*)-one derivatives (23–29). The ^1H NMR spectra showed the arylidene protons as singlet signals appearing at δ 7.20–8.64 ppm confirming their proposed structures. Scheme 2 illustrates the synthesis of ethyl benzothiazole-2-carboxylate (32) through the interaction of *o*-aminothiophenol (30) with diethyl oxalate (31). Compound 32 was reacted with hydrazine hydrate to obtain the corresponding acid hydrazide (33) which was utilized as a synthetic precursor for the preparation of different hydrazone derivatives (35–41) through the reaction with a collection of aromatic and heteroaromatic aldehydes (16, 18–22, 34) in refluxing glacial acetic acid. The ^1H NMR spectra of the

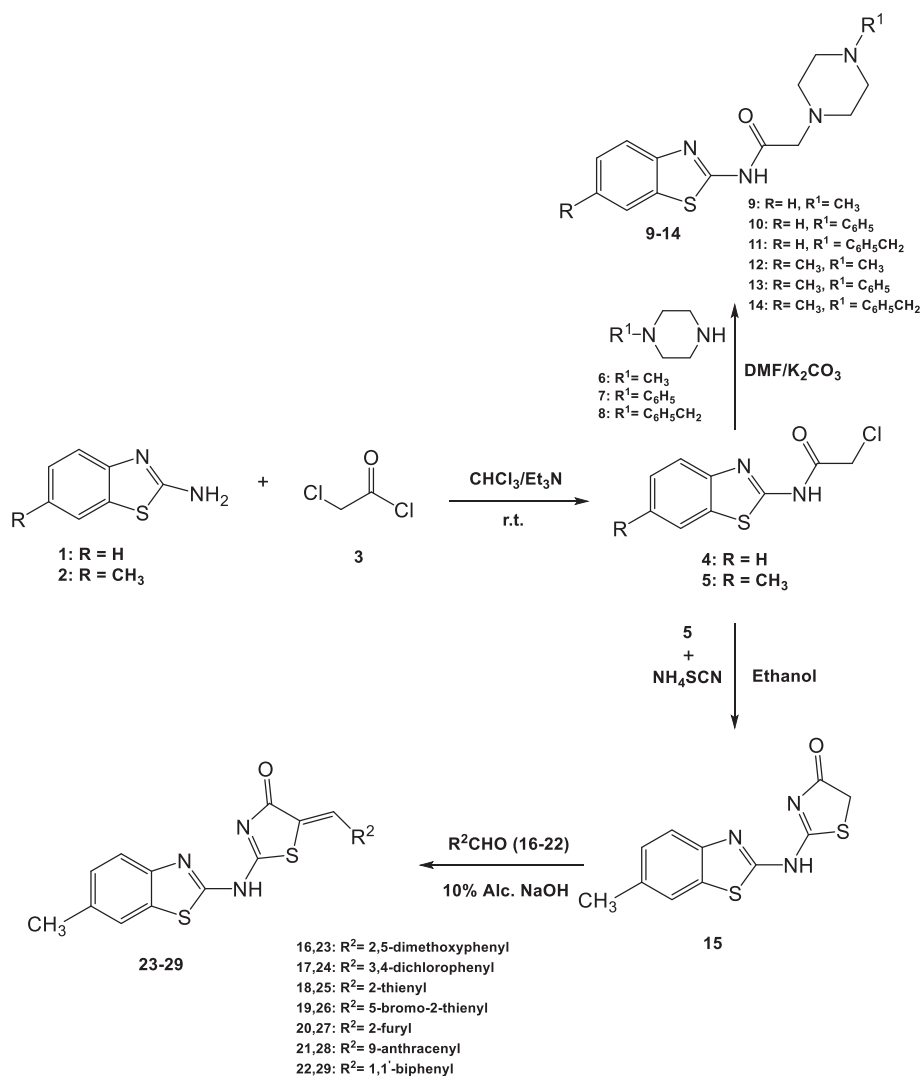
obtained hydrazone derivatives agreed with their suggested structures, showing the $\text{N}=\text{CH}$ proton as singlet signal at δ 8.54–8.99 ppm.

Scheme 3 describes the synthesis of groups of derivatives utilizing the acid hydrazide 33 as a key compound. Compounds 44 and 45 were obtained through the interaction of 33 with either 4-chloro or 4-fluorobenzoyl chloride (42 and 43 respectively) in glacial acetic acid. Appearance of additional aromatic signals due to the phenyl ring of acyl chloride in their ^1H NMR spectra proved their assigned structures. Under the same reaction conditions, compound 33 was reacted with a variety of isothiocyanate derivatives (46–49) to yield the corresponding thiosemicarbazides 50–53. The structures of the latter compounds were confirmed by the spectral data that showed the appearance of three singlet peaks due to NHNHCNSNH at $\delta > 9.41$ ppm in their ^1H NMR spectra. Additionally, the singlet peaks of tolyl CH_3 and the OCH_3 protons at δ 2.26 and 3.73 ppm confirmed the structure of the produced compounds 50 and 52 respectively. The thiosemicarbazides 50–53 underwent cyclization into their corresponding 1,2,4-triazole-3-thiols 54–57 through refluxing in 2 N NaOH. The disappearance of the three NH protons in the ^1H NMR spectra confirmed the success of the cyclization process. Finally, the sulfonamide derivatives 60 and 61 were obtained through the interaction of compound 33 with 4-bromobenzenesulfonyl chloride 58 and tosyl chloride 59 in glacial acetic acid. Their ^1H NMR spectrum showed the appearance of doublet signals corresponding to phenyl ring of *p*-substituted benzenesulfonyl group, in addition to the mass spectrum showing the molecular ion peak matching its molecular weight. Meanwhile, compound 61 was additionally proved by the appearance of the tolyl CH_3 protons as a singlet peak at δ 2.37 ppm.

2.2. Biological evaluation

2.2.1. In vitro antitumor activity

The antitumor activity of the synthesized compounds was assessed by determining their inhibitory effects on the cell growth of five cell



Scheme 1. Synthesis of compounds 9–14 and 23–29.

lines; namely hepatocellular carcinoma (HepG2), colorectal carcinoma (HCT-116), mammary gland cancer (MCF-7), prostate cancer (PC-3), and epithelioid carcinoma (HeLa) using the MTT assay. This colorimetric assay is based on the conversion of the yellow tetrazolium bromide (MTT) to a purple formazan derivative by mitochondrial succinate dehydrogenase in viable cells [10,11]. Different concentrations of the test compounds were used (100, 50, 25, 12.5, 6.25, 3.125, 1.56 μM). The percentage inhibition of the tested compounds at a concentration of 12.5 μM was used as the closest concentration to the NCI assay protocol. The mentioned values and IC₅₀ values in addition to those of lapatinib as a reference drug, are illustrated in Table 1. The results (Table 1) revealed that the most active antitumor compounds were 39, 40, 51, 56, and 61 with % inhibition values ranging from 50.7 to 73.1%. Furthermore, the IC₅₀ values of these active compounds are comparable to the reference drug lapatinib with values ranging from 3.26 to 12.3 (μM). By taking a closer look to the obtained results, it was found that compound 39 represents the most active compound among the active ones with the highest inhibition range values of 66.2–73.1% and lowest IC₅₀ value of 3.26–7.08 μM .

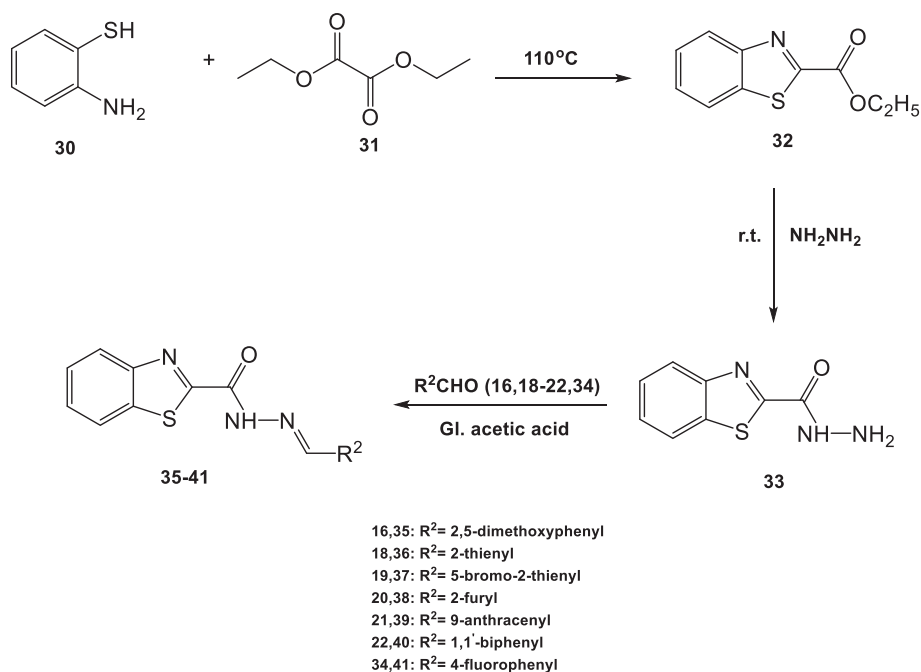
2.2.2. EGFR kinase activity assay

In order to investigate the mode of antitumor activity of the synthesized compounds, the most active ten compounds were further subjected to EGFR kinase activity assay [12,13]. % Inhibition at four different concentrations; 10, 100, 1000, and 10000 ng/ml, in addition

to IC₅₀ values of the tested compounds against lapatinib as a reference drug are shown in Table 2. Results obtained revealed that all the tested compounds exhibited high % inhibition values against EGFR ranging from 70.6 to 86.2% in concentration of 1 $\mu\text{g/ml}$, and range of 86.7–94.9% in concentration of 10 $\mu\text{g/ml}$ which is very close to the standard drug used. Additionally, results also confirmed that the most active antitumor compounds 39 and 40 exerted the highest potency through EGFR kinase inhibition, with IC₅₀ values of 24.58 and 30.42 nM, in comparison with 17.38 nM for lapatinib.

2.2.3. Cytotoxic activity against WI38 and A549 cell lines

Five of the most active compounds were selected to be further studied for their cytotoxic activity against human lung fibroblast cell line, WI38, as a normal cell line in order to test their safety. In addition, they were tested for their inhibitory activity on the human EGFR-positive non-small cell lung cancer cell line; A549. Lapatinib was used as a reference drug. The IC₅₀ values of the most active compounds against both cell lines are shown in Table 3. All these compounds exerted very high IC₅₀ values (42.8–73.2 μM) in comparison with lapatinib as a standard drug (13.6 μM) against the normal cell line WI38 demonstrating their safety. As for their cytotoxicity against the classic cell line A549, which is the human EGFR-positive NSCLC cell line, three of these most active compounds; 51, 39, and 40, exhibited inhibitory activity comparable to lapatinib, with IC₅₀ values of 5.41, 6.14, and 9.96 μM respectively vs. 5.48 μM for lapatinib. These cellular assay results are in



Scheme 2. Synthesis of compounds 35–41.

accordance with those of the enzyme assay proving the extreme potency of these most active compounds.

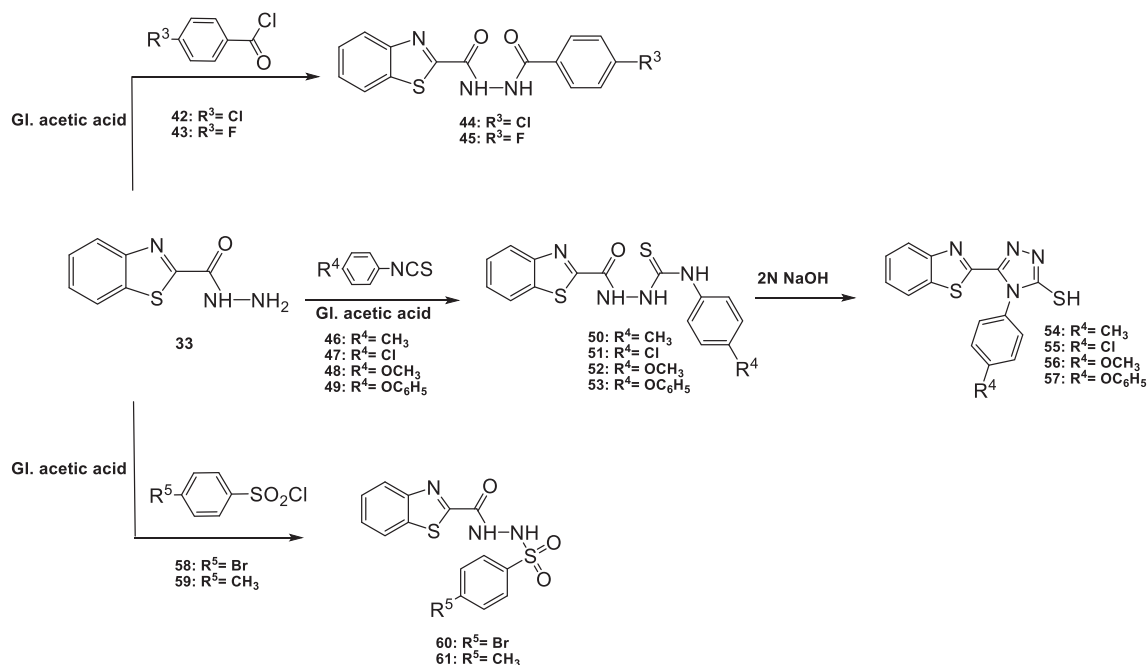
2.3. Molecular modeling studies

2.3.1. Docking into EGFR kinase

Molecular docking study was carried out to obtain a better understanding of EGFR higher inhibitory activity results of compounds **39**, **40**, **56** and **60**, in addition to rationalizing and describing their binding mode into EFGR active site. The most potent inhibitors were first subjected to conformational search study to get the best and least energy conformer of each compound that will be used for docking study (Fig. 2, [supplementary file](#)). Informative data about the binding orientations

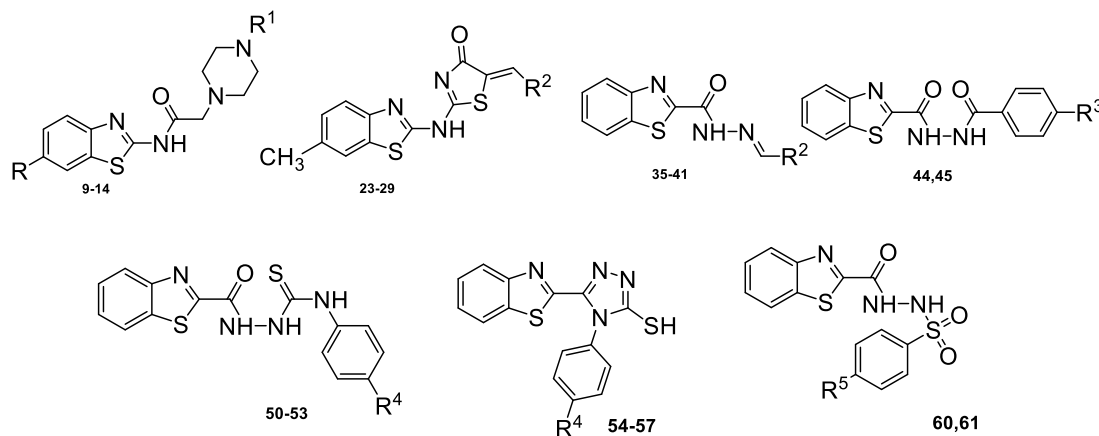
and interactions was obtained by docking of lapatinib [14] that was used as a reference ligand (95% inhibitory activity). It was cocrystallized in X-ray crystal structure in protein data bank using pdb 1xkk where it shows binding to Met793, Asp800 *via* hydrogen bonding interactions in addition to Phe856 residue, as well as the key amino acid residues of the active site, namely Lys745, Leu844, Met766 and Leu792 (Fig. 3).

Being docked in the active site of EGFR, compound **39** as the most active inhibitor (94.68% inhibition) fulfilled the key interactions, where the hydrogen bonding with Lys745 was established, as well as the Pi-cation interaction with Val726 residue at the active site of EGFR enzyme (Fig. 4). It was found that compound **40**, which showed 94.14% inhibition to EFGR compared to lapatinib, has shown the same pattern



Scheme 3. Synthesis of compounds 44, 45, 50–57, 60 and 61.

Table 1
% Inhibition and *in vitro* cytotoxicity (IC₅₀, μM) of the target compounds.



Comp.	% Inhibition					<i>In vitro</i> Cytotoxicity IC ₅₀ (μM)				
	HepG2	HCT-116	MCF-7	PC3	Hela	HepG2	HCT-116	MCF-7	PC3	Hela
9	17.6	30.4	13.9	< 10	25.2	71.27±4.0	43.46±3.1	69.83±4.5	83.43±4.8	55.71±3.7
10	45.3	63.9	52.9	47.2	61.4	17.56±1.6	9.65±0.9	13.89±1.2	24.34±1.9	9.09±0.9
11	< 10	16.4	14.8	< 10	< 10	80.09±4.3	65.29±3.8	83.20±4.9	>100	91.68±4.8
12	44.7	57.3	46.3	30.1	48.1	23.53±1.9	13.15±1.2	18.23±1.5	29.76±2.3	16.58±1.4
13	< 10	14.8	< 10	< 10	< 10	93.74±4.9	75.54±4.2	89.29±5.1	>100	>100
14	29.3	35.1	28.7	17.0	30.7	53.30±3.5	34.31±2.8	53.24±3.6	64.36±3.9	40.87±3.0
23	47.3	50.3	52.4	22.7	49.2	18.86±1.6	16.07±1.4	16.62±1.3	52.80±3.5	20.14±1.8
24	32.0	47.1	28.8	29.7	31.2	37.36±2.5	21.01±1.8	38.66±2.6	48.54±3.4	27.36±2.3
25	20.7	23.0	16.8	< 10	< 10	66.52±3.8	55.91±3.3	67.67±4.2	90.09±5.2	63.31±3.9
26	31.8	32.7	28.0	18.5	25.1	40.42±2.8	38.84±2.7	46.03±3.2	78.08±4.6	51.42±3.5
27	53.8	58.3	65.5	42.8	55.0	14.36±1.3	10.92±1.0	10.69±1.1	25.78±2.1	11.67±1.0
28	22.7	37.2	< 10	17.6	31.9	57.75±3.6	30.24±2.7	62.17±3.9	73.68±4.4	37.89±2.8
29	63.7	48.4	41.9	32.7	40.9	28.88±2.1	18.03±1.5	25.43±1.7	35.05±2.6	22.57±1.9
35	58.4	62.4	60.6	47.8	64.8	12.44±1.1	9.29±0.7	9.33±0.9	18.36±1.4	7.83±0.8
36	25.3	38.1	22.7	24.9	37.1	47.81±3.3	28.32±2.3	51.84±3.4	57.33±3.7	33.11±2.5
37	17.3	20.8	16.4	< 10	18.1	76.72±4.2	60.72±3.4	77.50±4.8	>100	79.18±4.2
38	31.6	49.3	39.0	30.2	36.2	33.20±2.3	22.08±2.0	32.68±2.1	42.53±2.9	30.20±2.3
39	68.1	73.1	66.2	69.3	66.4	7.08±0.6	3.26±0.2	6.95±0.5	5.87±0.5	6.12±0.7
40	65.4	71.0	66.3	60.2	66.1	8.59±0.7	4.56±0.3	8.16±0.8	12.30±1.1	7.80±0.8
41	< 10	< 10	< 10	< 10	< 10	>100	85.27±4.5	92.47±5.4	>100	>100
44	22.9	18.4	16.4	17.3	19.3	53.34±3.5	84.00±4.2	74.99±3.9	73.54±4.1	67.35±4.0
45	20.4	17.1	14.1	10	21.4	70.94±3.8	68.85±3.7	75.64±4.2	90.64±4.7	55.88±3.7
50	52.7	25.5	59.1	31.8	34.7	13.55±1.1	35.29±2.5	14.18±1.3	38.53±2.7	30.96±2.6
51	68.8	69.5	65.8	61.8	63.8	7.33±0.5	5.78±0.4	6.15±0.7	9.25±0.8	8.22±0.7
52	45.0	40.2	46.2	39.6	48.1	19.04±1.6	22.55±1.7	17.62±1.5	29.15±2.4	24.03±1.9
53	35.6	34.8	31.9	30.1	41.8	32.39±2.5	27.22±2.0	40.43±2.8	55.28±3.6	24.84±2.1
54	29.9	20.8	28.3	18.2	23.0	37.68±2.9	63.20±3.7	46.68±3.2	71.76±3.9	45.44±3.5
55	31.5	23.2	10	16.0	30.5	43.57±3.2	56.26±3.4	61.29±3.7	66.00±3.8	37.24±3.2
56	68.9	75.3	70.4	66.9	65.3	5.41±0.3	3.85±0.2	5.63±0.4	6.99±0.5	7.75±0.6
57	33.8	29.7	44.5	24.6	26.6	29.53±2.3	42.62±3.0	20.36±1.9	50.05±3.4	33.67±2.8
60	61.9	50.7	63.8	43.4	51.7	9.57±0.9	16.87±1.3	10.40±1.0	21.58±1.7	15.29±1.4
61	63.1	57.1	62.8	59.8	61.5	8.51±0.7	10.98±0.9	9.20±0.8	12.11±1.1	11.02±1.0
Lapatinib	86.4	91.8	89.7	90.6	97.3	5.13±3.1	6.34±4.0	5.71±3.5	4.29±1.7	3.39±2.7

of binding type as the reference ligand as follows; hydrogen bonding via Lys745 and Pi-cation by Leu844 and Cys797 interactions which may interpret its higher activity, (Fig. 4). Compound 56 (86.75%) showed hydrogen bonding with Met793 and Leu792 via thiocarbonyl sulfur atom. Moreover it was engaged in a second hydrogen bond with the side chain Arg841 by sulfur heteroatom of thiazole ring, and an additional cationic arene interaction had been noticed with triazole ring with Val726 (Fig. 5). The 2D binding model of compound 60 (87%) into

EGFR was depicted in Fig. 5, where hydrogen bonding interactions were mediated via carbonyl oxygen atom to Lys745 and Met 766, in addition to arene-cationic interaction to Val726 through thiazole ring counterpart which may cause higher activity of compound 60 into EGFR.

The core structures under concern adopted the same orientation as the reference compound, that was clarified by taking compound 39 as an example where both compound 39 and lapatinib have been

Table 2
% Inhibition and IC₅₀ (nM) of EGFR kinase assay kit for the target compounds.

Comp.	% Inhibition (ng/ml)				IC ₅₀ (nM)
	10	100	1000	10000	
10	27.7	49.8	76.0	93.4	94.73 ± 2.7
23	30.6	61.1	78.2	92.0	53.96 ± 1.5
27	25.5	50.4	72.7	89.8	113.35 ± 3.2
35	32.0	54.0	72.5	92.5	73.04 ± 2.1
39	41.3	63.1	79.2	94.7	24.58 ± 0.7
40	34.7	65.7	86.3	94.1	30.42 ± 0.9
51	37.1	66.2	77.8	92.9	29.31 ± 0.8
56	12.7	44.8	69.0	86.8	232.51 ± 6.6
60	10.2	44.1	70.6	87.0	241.62 ± 6.9
61	36.4	61.8	75.4	90.6	38.81 ± 1.1
Lapatinib	39.7	70.6	85.9	95.0	17.38 ± 0.4

Table 3
IC₅₀ (μM) of the most active compounds against WI38 and A549 cell lines.

Comp.	WI38	A549
10	54.2 ± 3.2	18.4 ± 1.03
35	42.8 ± 2.9	47.4 ± 2.66
39	65.0 ± 3.8	6.14 ± 0.34
40	61.8 ± 3.47	9.96 ± 0.56
51	73.2 ± 4.1	5.41 ± 0.3
Lapatinib	13.6 ± 0.76	5.48 ± 0.31

completely superimposed in the active site center (Fig. 6) which may contribute to the higher potency of the tested compound to be as potent as lapatinib reference.

A respected point of view was to compare the shape of the docked compounds into the active site of ATP site of EGFR. Fig. 7 clearly shows all active compounds of interest, namely 39, 40, 56, and 60 were deeply buried into the active site and fulfilling its cavity completely which in turn has its impact on their higher inhibitory activity on EGFR enzyme.

2.3.2. Surface mapping

In a further step for rationalizing the activity of tested compounds, surface mapping calculations were conducted for compounds 39, 40, 56, and 60 which showed the best EGFR inhibitory profile in this study. Fig. 8 pointed out a uniform distribution of hydrophobic regions in a similar manner between all tested derivatives giving more lipophilic

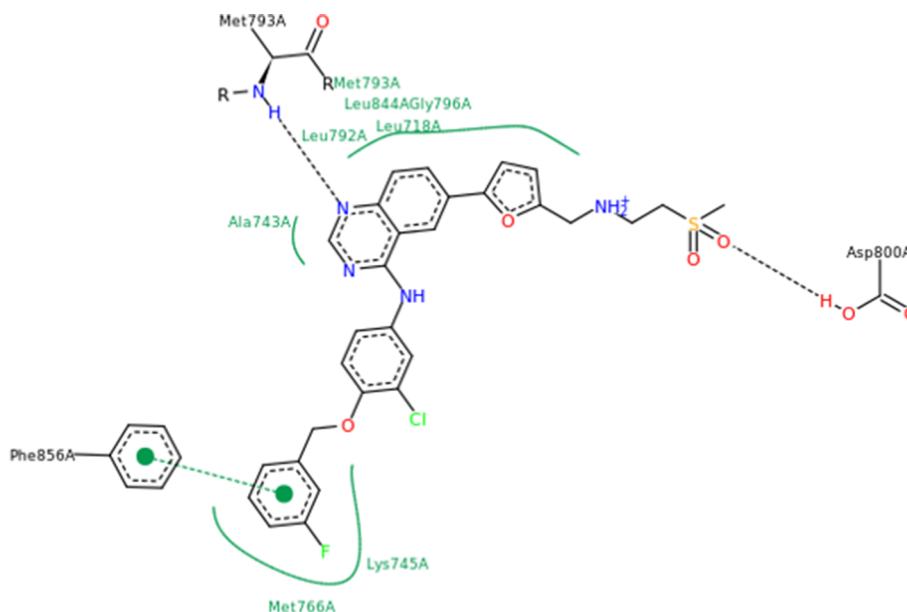


Fig. 3. Close-up view of binding of ligand (lapatinib) at binding pocket of EGFR X-ray crystal structure (pdb 1xkk).

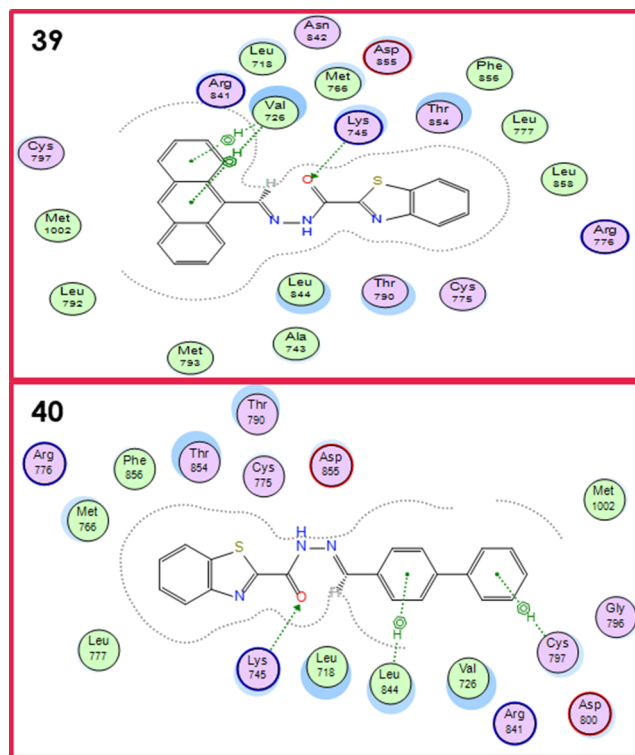


Fig. 4. 2D Binding mode and residues involved in the recognition of active compounds 39 and 40 at active site of EGFR.

character of the molecule which is responsible for interaction with the enzyme. A deep interaction with the hydrophobic pocket is suggested at ATP binding back site that could be in charge for perfect fitting at active site. In conclusion, our modeling studies were in good accordance with the experimental results and supported them with visual evidences and explanations too.

2.4. Structure-activity correlation

Based on the obtained results, it was revealed that in general the unsubstituted benzothiazole derivatives are more active than the

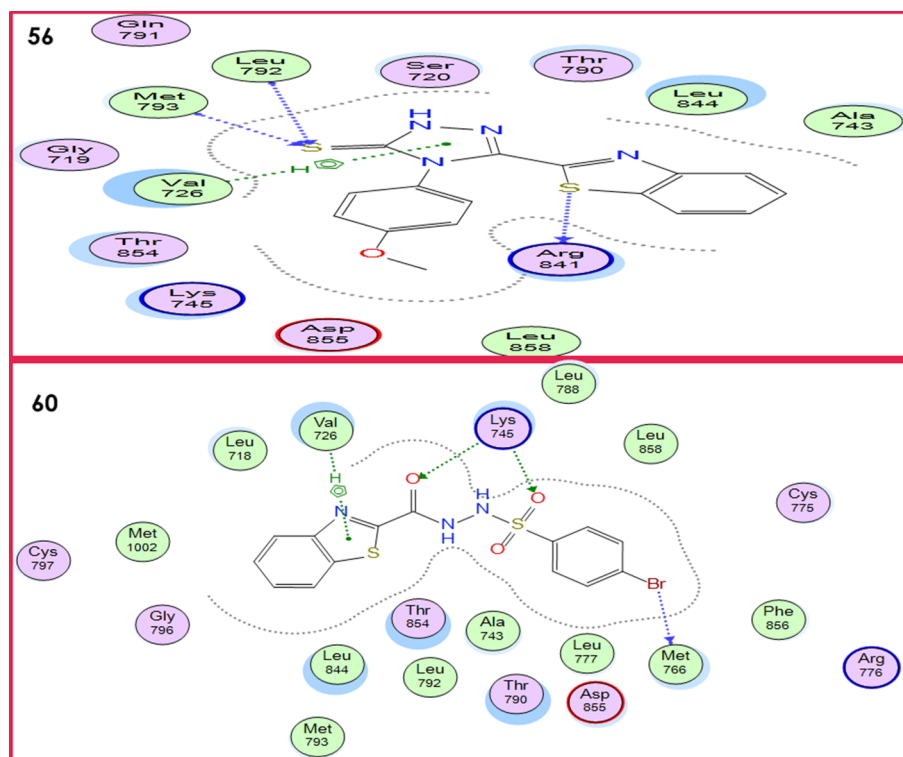


Fig. 5. 2D Binding mode and residues involved in the recognition of active compounds 56 and 60 at active site of EGFR.

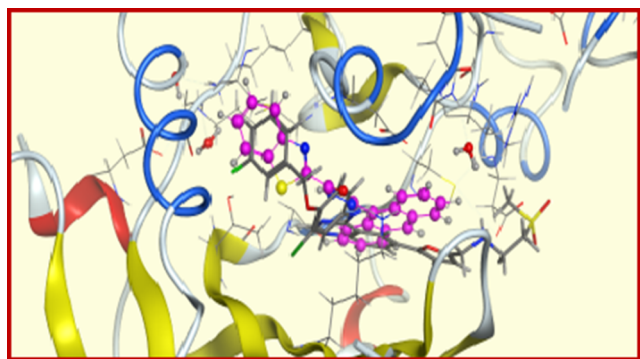


Fig. 6. 3D Overview of compound 39 (pink) overlay with lapatinib reference ligand at binding site of EGFR. (For interpretation of the references to colour in this figure legend, the reader is referred to the web version of this article.)

methyl ones among the synthesized compounds. This was obvious through the % inhibition assay against the selected tumor cell lines and the % inhibition against EGFR kinase enzyme. The consistency of the results revealed that such compounds are active as antitumor agents and they act through the inhibition of EGFR kinase enzyme. Taking a closer look for the active unsubstituted derivatives, it was found that the presence of the acetamido structure and the thiazole-4(5*H*)-one moiety doesn't favor the activity, while the presence of the acid hydrazide group is very essential for activity. Specifically, the acid hydrazide group appeared in the most active compounds, viz. 39 and 40. Furthermore, the presence of polycyclic ring system such as anthracene and biphenyl group increases the activity of the compounds as in case of compounds 39 and 40. It seems that bulkiness of substituents in vicinity of the 2-position of the benzothiazole ring accounts for the activity of these compounds. Moreover, compounds 23 and 35, each of which contains a dimethoxyphenyl group, revealed activity which emphasizes the role played by the steric factor. On the other hand, the presence of

electron withdrawing group is also characteristic for activity more than the electron donating groups as in case of compounds 56 and 61.

3. Conclusion

In the present study, different series of benzothiazole-based derivatives were synthesized. The most active antitumor compounds were the acid hydrazones 39 and 40 which also represented the most potent inhibitors to EGFR with % inhibition values ranging from 60.2 to 73.1% and with IC_{50} values of 24.58 and 30.42 nM respectively in comparison with 17.38 nM for lapatinib as a standard drug. Docking studies into EGFR active site revealed that compounds 39 and 40 showed a pattern of binding similar to lapatinib as the reference ligand as they fulfilled the key interactions, where the hydrogen bonding with Lys745 was established. Compounds of interest, namely 39 and 40, were deeply buried into the active site and completely housed in its cavity which in turn has its impact on their higher inhibitory activity on EGFR enzyme. Surface mapping displayed a deep interaction with the hydrophobic pocket at ATP binding back site that could be in charge for perfect fitting at active site.

4. Experimental protocols

The synthesis of the designed compounds was performed in the Department of Medicinal Chemistry, Faculty of Pharmacy, Mansoura University, Mansoura, Egypt. The antitumor activity assay and cytotoxicity against WI38 normal cell line were conducted in the Department of Pharmacognosy, Faculty of Pharmacy, Mansoura University, Mansoura, Egypt. EGFR inhibitory assay and cytotoxicity against A549 cell line were conducted at the confirmatory diagnostic unit, VACSERA, Egypt. Melting points ($^{\circ}C$) were determined on Stuart melting point apparatus and are uncorrected. 1H , ^{13}C NMR were recorded on a Joel 500 MHz FT spectrometer and Bruker 400 MHz spectrometer; chemical shifts are expressed in δ ppm with reference to TMS. Mass spectral (MS) data were obtained on direct inlet part to mass analyzer in thermo scientific GCMS model ISQ at the Regional Center

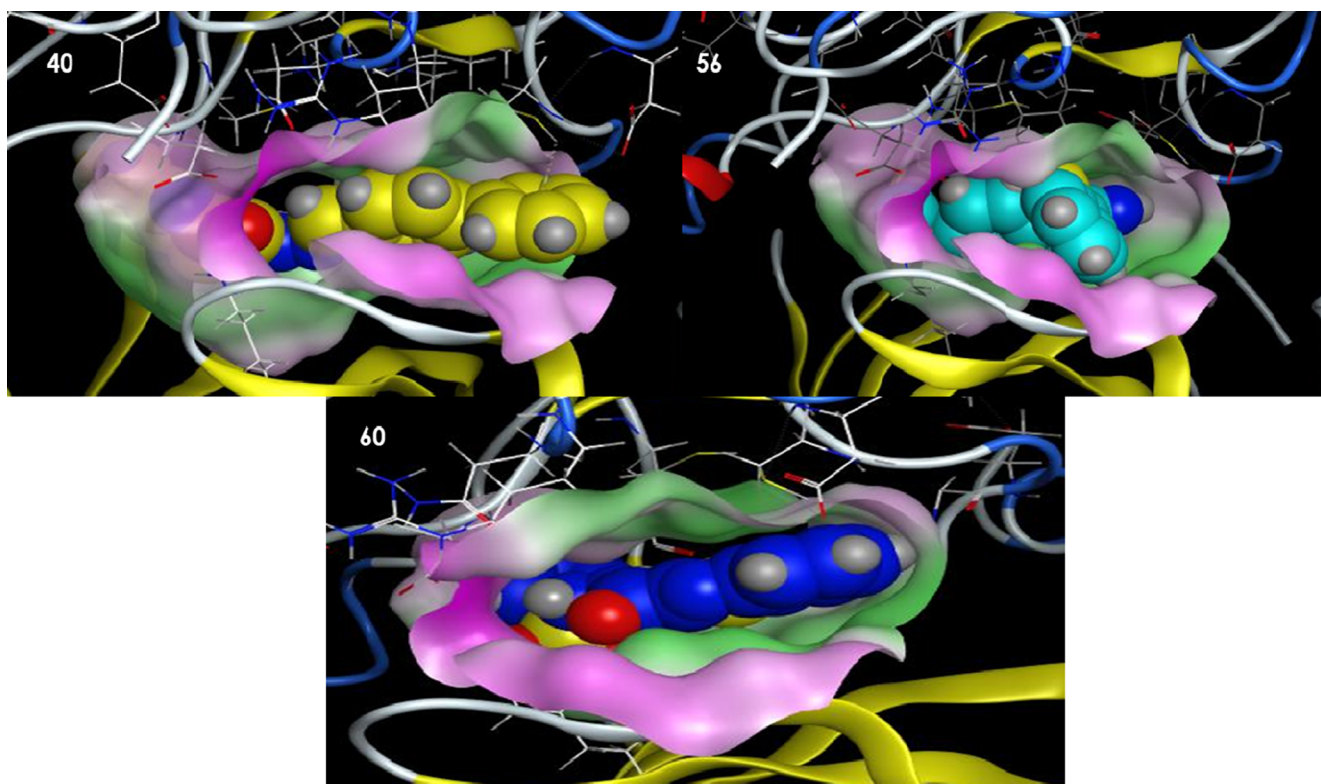


Fig. 7. 3D View of active candidates 40, 56 and 60 deep buried into the pocket of EGFR (surface map).

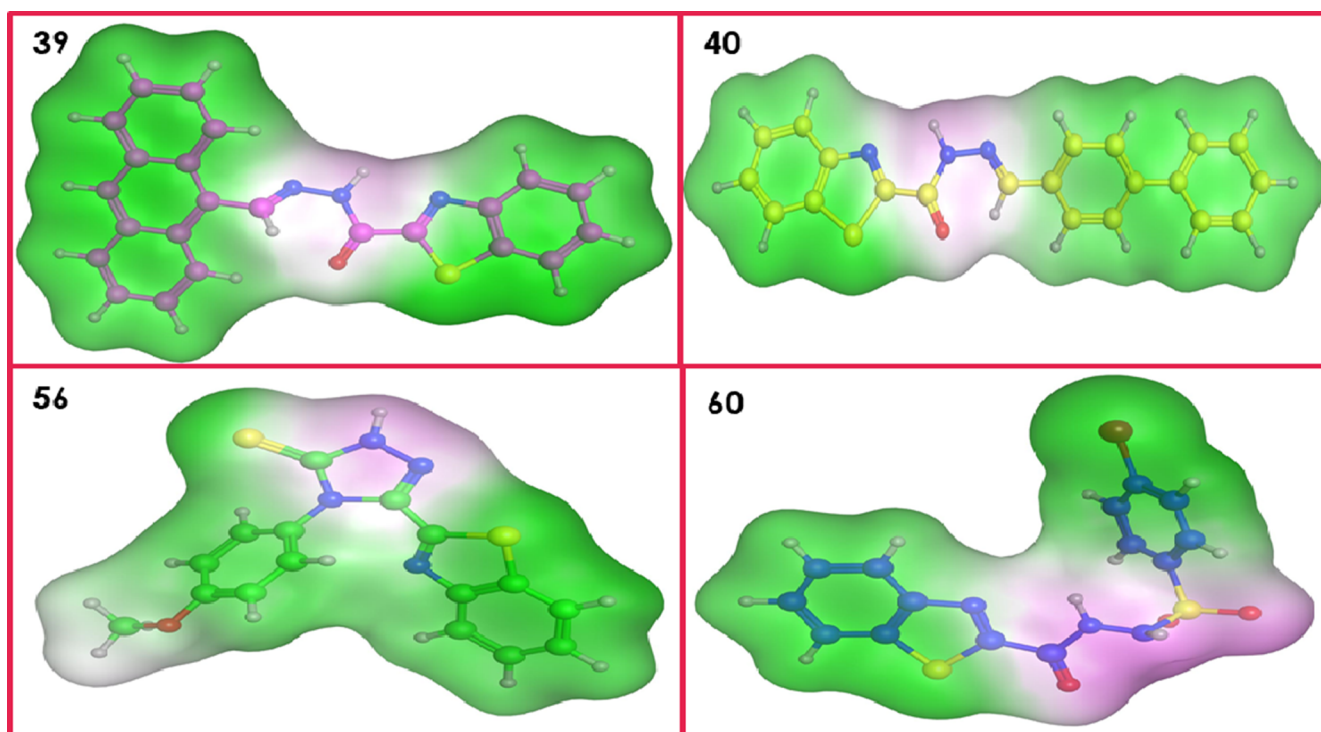


Fig. 8. Surface map for active compounds 39, 40, 56, and 60. Pink: hydrogen bond, white: mild polar, green: hydrophobic. (For interpretation of the references to colour in this figure legend, the reader is referred to the web version of this article.)

for Mycology and Biotechnology (RCMB), Al-Azhar University, Cairo, Egypt. Thin layer chromatography was performed on precoated (0.25 mm) silica gel GF₂₅₄ plates (E. Merck, Germany), compounds were detected with 254 nm UV lamp. All the fine chemicals and reagents used were purchased from Aldrich Chemicals Co, USA. Compounds **4** [15], **5** [16], **9** [17], **10**, **11** [18], **15** [19], **32**, **33** [20], **44** [21], **51**, **52**, **55**, **56** [22] were previously reported.

4.1. Chemistry

4.1.1. Synthesis of *N*-(benzo[d]thiazol-2-yl)-2-chloroacetamides (**4** and **5**)

To a solution of the appropriate aminobenzothiazole (**1** or **2**, 0.01 mol) and triethylamine (5.6 ml, 0.04 mol) in chloroform (50 ml), chloroacetyl chloride (**3**, 3.18 ml, 0.04 mol) was added slowly. The reaction mixture was stirred at room temperature for 2 h. The precipitate formed was filtered, washed with water, and recrystallized from ethanol to afford the chloroacetamide derivatives **4** and **5**.

4: Yellowish white crystals, yield %: 88, m.p.: 200 °C (char.) (reported m.p. 140–143 °C) [15].

5: Greenish brown crystals, yield %: 91, m.p.: 180–182 °C (reported m.p. 174–176 °C) [16].

4.1.2. Synthesis of *N*-(benzo[d]thiazol-2-yl)-2-((4-substituted)piperazin-1-yl)acetamides (**9**–**14**)

A mixture of the chloroacetamide derivative (**4** or **5**, 0.002 mol), potassium carbonate (2.21 g, 0.016 mol), and the appropriate piperazine (**6**–**8**, 0.002 mol) in DMF (25 ml) was stirred at 50 °C for 6 h. The precipitate formed was filtered, washed with water, and recrystallized from ethanol to obtain the piperazine derivatives **9**–**14**.

9: White crystals, yield %: 38, m.p.: 280–282 °C (reported m.p. 257 °C) [17].

10: White crystals, yield %: 48, m.p.: 180–182 °C (reported m.p. 184–186 °C) [18].

11: White crystals, yield %: 46, m.p.: 140–142 °C (reported m.p. 118–119 °C) [18].

12: White crystals, yield %: 47, m.p.: 208–210 °C. ¹H NMR (CDCl₃): δ 2.33 (s, 3H, piperazine-CH₃), 2.47 (s, 3H, benzothiazole-CH₃), 2.53 (br s, 4H, piperazine-H), 2.68 (br s, 4H, piperazine-H), 3.28 (s, 2H, COCH₂), 7.25 (d, 1H, *J* = 7.5 Hz, Ar-H), 7.61 (s, 1H, Ar-H), 7.68 (d, 1H, *J* = 8.0 Hz, Ar-H), 10.38 (s, 1H, NH). ¹³C NMR (CDCl₃): δ 21.4, 45.9, 53.6, 54.9, 61.0, 120.5, 121.2, 127.7, 132.3, 134.0, 146.4, 156.3, 169.0. MS (*m/z*, %): (M⁺ 304.28, 14.69), (M⁺ + 1 305.30, 3.13), 70.08 (100.00). Analysis calculated for C₁₅H₂₀N₄O₂S: C, 59.18; H, 6.62; N, 18.41.

13: White crystals, yield %: 79, m.p.: 198–200 °C. ¹H NMR (CDCl₃): δ 2.43 (s, 3H, CH₃), 2.80 (s, 4H, piperazine-H), 3.26 (s, 4H, piperazine-H), 3.35 (s, 2H, COCH₂), 6.86–6.92 (m, 4H, Ar-H), 7.21–7.27 (m, 2H, Ar-H), 7.57 (s, 1H, Ar-H), 7.63 (d, 1H, *J* = 8.5 Hz, Ar-H), 9.95 (s, 1H, NH). ¹³C NMR (CDCl₃): δ 21.4, 49.1, 53.5, 61.0, 116.4, 120.3, 120.5, 121.1, 127.7, 129.1, 132.2, 134.0, 146.2, 150.7, 156.2, 168.6. MS (*m/z*, %): (M⁺ 366.30, 100.00), (M⁺ + 1 367.34, 24.31). Analysis calculated for C₂₀H₂₂N₄O₂S: C, 65.55; H, 6.05; N, 15.29.

14: White crystals, yield %: 63, m.p.: 234–236 °C. ¹H NMR (CDCl₃): δ 2.47 (s, 3H, CH₃), 2.56 (br s, 4H, piperazine-H), 2.66 (s, 4H, piperazine-H), 3.27 (s, 2H, COCH₂), 3.55 (s, 2H, CH₂-Ph), 7.25–7.28 (m, 2H, Ar-H), 7.32–7.33 (m, 4H, Ar-H), 7.61 (s, 1H, Ar-H), 7.68 (d, 1H, *J* = 8.0 Hz, Ar-H), 10.41 (s, 1H, NH). ¹³C NMR (CDCl₃): δ 21.4, 43.5, 49.4, 60.8, 62.6, 120.5, 121.2, 127.7, 128.4, 128.5, 129.0, 146.2, 156.3, 168.8. MS (*m/z*, %): (M⁺ 380.32, 100.00), (M⁺ + 1 381.37, 26.22). Analysis calculated for C₂₁H₂₄N₄O₂S: C, 66.29; H, 6.36; N, 14.72.

4.1.3. Synthesis of 2-((6-methyl-benzo[d]thiazol-2-yl)amino)thiazol-4(5H)-one (**15**)

A mixture of compound **5** (1.20 g, 0.005 mol) and ammonium thiocyanate (1.52 g, 0.02 mol) in ethanol (50 ml) was heated under

reflux for 24 h. The obtained precipitate was filtered, washed with water and recrystallized from ethanol. Reddish white crystals, yield %: 87, m.p.: 250–252 °C (reported m.p. 243–245 °C) [19].

4.1.4. Synthesis of 5-arylidene-2-((6-methylbenzo[d]thiazol-2-yl)amino)thiazol-4(5H)-ones (**23**–**29**)

To a solution of compound **15** (0.24 g, 0.001 mol) in 10% ethanolic sodium hydroxide (1 g sodium hydroxide in 10 ml 96% ethanol), the appropriate aldehyde (**16**–**22**) (0.001 mol) was added and the reaction mixture was stirred at room temperature for about 10 min. The precipitate formed was filtered, washed with water and recrystallized from the appropriate solvent (ethanol or chloroform).

23: Reddish brown crystals, yield %: 92, m.p.: 283–285 °C. ¹H NMR (DMSO-*d*₆): δ 2.36 (s, 3H, CH₃), 3.76 (s, 3H, OCH₃), 3.81 (s, 3H, OCH₃), 6.93 (d, 1H, *J* = 7.5 Hz, Ar-H), 7.01 (d, 1H, *J* = 8.5 Hz, Ar-H), 7.07–7.10 (m, 2H, Ar-H), 7.47 (d, 1H, *J* = 8.0 Hz, Ar-H), 7.56 (s, 1H, Ar-H), 7.70 (s, 1H, =CH). ¹³C NMR (DMSO-*d*₆): δ 21.0, 55.4, 56.0, 112.4, 112.6, 112.8, 114.7, 118.8, 119.8, 120.8, 124.7, 126.3, 131.4, 133.1, 134.6, 148.5, 151.9, 153.1, 180.3. MS (*m/z*, %): (M⁺ 411.31, 6.60), (M⁺ + 1 412.33, 3.01), 394.24 (100.00). Analysis calculated for C₂₀H₁₇N₃O₃S₂: C, 58.38; H, 4.16; N, 10.21.

24: Reddish brown crystals, yield %: 94, m.p.: 338–340 °C. ¹H NMR (DMSO-*d*₆): δ 2.37 (s, 3H, CH₃), 3.37 (s, 1H, NH), 7.10 (dd, 1H, *J* = 1.0 Hz, *J* = 9.0 Hz, Ar-H), 7.40 (s, 1H, =CH), 7.49 (d, 1H, *J* = 8.5 Hz, Ar-H), 7.55–7.57 (m, 2H, Ar-H), 7.74 (d, 1H, *J* = 8.0 Hz, Ar-H), 7.81 (d, 1H, *J* = 2.5 Hz, Ar-H). ¹³C NMR: δ 21.0, 69.7, 119.9, 120.8, 121.9, 126.3, 128.4, 130.2, 130.8, 131.1, 131.6, 135.5, 136.4. MS (*m/z*, %): (M⁺ 420.40, 13.65), (M⁺ + 1 421.64, 10.81), (M⁺ + 2 422.86, 5.19), 57.19 (100.00). Analysis calculated for C₁₈H₁₁Cl₂N₃O₂S: C, 51.44; H, 2.64; N, 10.00.

25: Reddish brown crystals, yield %: 93, m.p.: 298–300 °C. ¹H NMR (DMSO-*d*₆): δ 2.36 (s, 3H, CH₃), 3.40 (s, 1H, NH), 7.09 (d, 1H, *J* = 8.0 Hz, Ar-H), 7.18 (t, 1H, *J* = 4.0 Hz, Ar-H), 7.42 (d, 1H, *J* = 3.0 Hz, Ar-H), 7.48 (d, 1H, *J* = 8.0 Hz, Ar-H), 7.56 (s, 1H, Ar-H), 7.62 (s, 1H, =CH), 7.75 (d, 1H, *J* = 5.5 Hz, Ar-H). MS (*m/z*, %): (M⁺ 357.19, 74.63), (M⁺ + 1 358.11, 18.57), 311.21 (100.00). Analysis calculated for C₁₆H₁₁N₃O₃S: C, 53.76; H, 3.10; N, 11.76.

26: Reddish brown crystals, yield %: 94, m.p.: 335–337 °C. ¹H NMR (DMSO-*d*₆): δ 2.36 (s, 3H, CH₃), 3.37 (s, 1H, NH), 7.09 (d, 1H, *J* = 8.5 Hz, Ar-H), 7.27 (d, 1H, *J* = 4.0 Hz, Ar-H), 7.31 (d, 1H, *J* = 4.0 Hz, Ar-H), 7.49 (d, 1H, *J* = 8.0 Hz, Ar-H), 7.55 (s, 1H, =CH), 7.57 (s, 1H, Ar-H). ¹³C NMR: δ 21.0, 114.3, 117.0, 119.9, 120.8, 126.3, 130.8, 131.5, 131.7, 132.7, 142.5. MS (*m/z*, %): (M⁺ 436.55, 12.22), (M⁺ + 1 437.59, 4.30), 90.93 (100.00). Analysis calculated for C₁₆H₁₀BrN₃O₃S: C, 44.04; H, 2.31; N, 9.63.

27: Reddish brown crystals, yield %: 93, m.p.: 308–310 °C. ¹H NMR (DMSO-*d*₆): δ 2.36 (s, 3H, CH₃), 3.37 (s, 1H, NH), 6.64 (dd, 1H, *J* = 2.0 Hz, *J* = 5.5 Hz, Ar-H), 6.74 (t, 1H, *J* = 3.5 Hz, Ar-H), 7.08 (dd, 1H, *J* = 1.5 Hz, *J* = 9.5 Hz, Ar-H), 7.20 (s, 1H, =CH), 7.46 (d, 1H, *J* = 8.5 Hz, Ar-H), 7.55 (s, 1H, Ar-H), 7.78 (d, 1H, *J* = 1.0 Hz, Ar-H). ¹³C NMR: δ 21.0, 111.9, 112.8, 113.2, 119.7, 120.7, 126.2, 131.1, 131.3, 144.7, 148.5, 151.2. MS (*m/z*, %): (M⁺ 341.20, 74.85), (M⁺ + 1 342.16, 38.31), 44.14 (100.00). Analysis calculated for C₁₆H₁₁N₃O₂S₂: C, 56.29; H, 3.25; N, 12.31.

28: Reddish brown crystals, yield %: 94, m.p.: 328–330 °C. ¹H NMR (DMSO-*d*₆): δ 2.35 (s, 3H, CH₃), 3.40 (s, 1H, NH), 7.05 (d, 1H, *J* = 7.5 Hz, Ar-H), 7.40 (d, 1H, *J* = 6.0 Hz, Ar-H), 7.54–7.58 (m, 5H, Ar-H), 8.01 (d, 2H, *J* = 10.0 Hz, Ar-H), 8.11–8.15 (m, 3H, Ar-H), 8.64 (s, 1H, =CH). ¹³C NMR: δ 21.0, 119.8, 120.7, 121.9, 125.5, 125.6, 126.2, 127.2, 127.9, 128.8, 130.9, 131.0, 131.4, 141.9. MS (*m/z*, %): (M⁺ 451.47, 12.02), 45.22 (100.00). Analysis calculated for C₂₆H₁₇N₃O₂S₂: C, 69.16; H, 3.79; N, 9.31.

29: Reddish brown crystals, yield %: 92, m.p.: 338–340 °C. ¹H NMR (DMSO-*d*₆): δ 2.37 (s, 3H, CH₃), 3.37 (s, 1H, NH), 7.10 (dd, 1H, *J* = 1.5 Hz, *J* = 9.5 Hz, Ar-H), 7.36–7.39 (m, 2H, Ar-H), 7.46–7.49 (m, 4H, Ar-H), 7.57 (s, 1H, =CH), 7.67 (d, 2H, *J* = 8.0 Hz, Ar-H),

7.71–7.74 (m, 3H, Ar-H). ^{13}C NMR: δ 21.0, 119.8, 120.7, 124.1, 126.2, 126.6, 126.8, 126.9, 127.1, 127.7, 129.0, 129.7, 131.4, 133.0, 134.5, 139.3, 139.7, 157.8. MS (m/z , %): (M^+ 427.67, 8.82), 43.31 (100.00). Analysis calculated for $\text{C}_{24}\text{H}_{17}\text{N}_3\text{O}_2$: C, 67.42; H, 4.01; N, 9.83.

4.1.5. Synthesis of ethyl benzothiazole-2-carboxylate (32)

A mixture of *o*-aminothiophenol (**30**, 1.06 ml, 0.01 mol) and diethyl oxalate (**31**, 4.38 ml, 0.03 mol) was heated at 110 °C for 4 h. The precipitate formed was filtered after cooling, then washed and recrystallized from petroleum ether. Greenish yellow needles, yield %: 84, m.p.: 68–70 °C as reported [20].

4.1.6. Synthesis of benzothiazole-2-carbohydrazide (33)

A mixture of compound **32** (1.9 gm, 0.01 mol) and hydrazine hydrate (5 ml, 0.1 mol) was stirred at room temperature for 10 min. The carbohydrazide formed was washed with water and recrystallized from ethanol [20]. Yellowish crystals, yield %: 91, m.p.: 200–202 °C (reported m.p. 172–174 °C) [20].

4.1.7. Synthesis of (E)-N'-(substituted arylidene)benzo[d]thiazole-2-carbohydrazides (35–41)

To a solution of compound **33** (0.193 g, 0.001 mol) in glacial acetic acid (10 ml), the appropriate aldehyde (**16**, **18–22**, **34**) (0.001 mol) was added and the reaction mixture was heated under reflux for 1 h. The precipitate formed was filtered on hot, washed with water and recrystallized from the appropriate solvent (ethanol or chloroform).

35: Greenish white crystals, yield %: 91, m.p.: 283–285 °C. ^1H NMR (DMSO- d_6): δ 3.75 (s, 3H, OCH_3), 3.81 (s, 3H, OCH_3), 7.02–7.07 (m, 2H, Ar-H), 7.37 (d, 1H, $J = 2.5$ Hz, Ar-H), 7.59–7.67 (m, 2H, Ar-H), 8.18 (d, 1H, $J = 8.0$ Hz, Ar-H), 8.26 (d, 1H, $J = 8.0$ Hz, Ar-H), 8.99 (s, 1H, N = CH). ^{13}C NMR: δ 55.4, 56.4, 109.3, 113.6, 118.1, 122.7, 123.0, 124.1, 127.1, 127.3, 136.0, 146.1, 152.6, 152.7, 153.2, 156.1, 163.7. MS (m/z , %): (M^+ 341.22, 100.00), ($\text{M}^+ + 1$ 342.28, 30.06). Analysis calculated for $\text{C}_{17}\text{H}_{15}\text{N}_3\text{O}_3\text{S}$: C, 59.81; H, 4.43; N, 12.31.

36: Brownish white crystals, yield % 89, m.p.: 198–200 °C. ^1H NMR (DMSO- d_6): δ 7.15 (d, 1H, $J = 4.0$ Hz, Ar-H), 7.46–7.70 (m, 4H, Ar-H), 8.18 (d, 1H, $J = 8.5$ Hz, Ar-H), 8.25 (d, 1H, $J = 7.5$ Hz, Ar-H), 8.85 (s, 1H, N = CH), 12.54 (s, 1H, NH). MS (m/z , %): (M^+ 287.10, 14.71), ($\text{M}^+ + 1$ 288.14, 2.29), 135.09 (100.00). Analysis calculated for $\text{C}_{13}\text{H}_9\text{N}_3\text{O}_2\text{S}$: C, 54.34; H, 3.16; N, 14.62.

37: Brownish white crystals, yield %: 93, m.p.: 248–250 °C. ^1H NMR (DMSO- d_6): δ 7.28 (d, 1H, $J = 3.5$ Hz, Ar-H), 7.32 (d, 1H, $J = 4.0$ Hz, Ar-H), 7.60–7.67 (m, 2H, Ar-H), 8.18 (d, 1H, $J = 7.5$ Hz, Ar-H), 8.26 (d, 1H, $J = 7.5$ Hz, Ar-H), 8.67 (s, 1H, N = CH), 12.40 (s, 1H, NH). ^{13}C NMR: 115.7, 123.1, 124.1, 127.2, 131.5, 132.5, 134.7, 136.0, 140.4, 145.0, 152.6, 155.9, 163.5. MS (m/z , %): (M^+ 366.00, 22.85), 213.09 (100.00). Analysis calculated for $\text{C}_{13}\text{H}_8\text{BrN}_3\text{O}_2\text{S}$: C, 42.63; H, 2.20; N, 11.47.

38: Brownish white crystals, yield %: 91, m.p.: 178–180 °C. ^1H NMR (DMSO- d_6): δ 6.66 (dd, 1H, $J = 2.0$ Hz, $J = 5.5$ Hz, Ar-H), 6.98 (d, 1H, $J = 3.5$ Hz, Ar-H), 7.59–7.67 (m, 2H, Ar-H), 7.88 (d, 1H, $J = 1.0$ Hz, Ar-H), 8.18 (d, 1H, $J = 7.5$ Hz, Ar-H), 8.26 (d, 1H, $J = 7.0$ Hz, Ar-H), 8.54 (s, 1H, N = CH), 12.69 (s, 1H, NH). ^{13}C NMR: δ 112.4, 114.5, 123.1, 124.0, 127.1, 127.3, 136.0, 139.8, 145.7, 149.2, 152.7, 156.0, 163.7. MS (m/z , %): (M^+ 271.20, 8.26), ($\text{M}^+ + 1$ 272.20, 1.87), 52.19 (100.00). Analysis calculated for $\text{C}_{13}\text{H}_9\text{N}_3\text{O}_2\text{S}$: C, 57.55; H, 3.34; N, 15.49.

39: Reddish brown crystals, yield %: 91, m.p.: 228–230 °C. ^1H NMR (DMSO- d_6): δ 7.58–7.70 (m, 7H, Ar-H), 8.17 (d, 2H, $J = 8.0$ Hz, Ar-H), 8.25 (d, 1H, $J = 7.5$ Hz, Ar-H), 8.30 (d, 1H, $J = 7.5$ Hz, Ar-H), 8.77 (s, 1H, N = CH), 8.82 (d, 2H, $J = 9.0$ Hz, Ar-H), 12.93 (s, 1H, NH). ^{13}C NMR: δ 123.2, 124.1, 124.6, 124.9, 125.6, 127.2, 127.4, 129.1, 129.1, 129.8, 130.2, 130.9, 150.1, 152.8, 156.1, 157.8, 163.7. MS (m/z , %): (M^+ 381.25, 100.00), ($\text{M}^+ + 1$ 382.29, 27.02). Analysis calculated for $\text{C}_{21}\text{H}_{15}\text{N}_3\text{O}_2\text{S}$: C, 70.57; H, 4.23; N, 11.76.

40: Reddish brown crystals, yield %: 89, m.p.: 343–345 °C. ^1H NMR (DMSO- d_6): δ 7.61–7.66 (m, 2H, Ar-H), 7.72–7.84 (m, 8H, Ar-H), 7.97 (d, 1H, $J = 9.0$ Hz, Ar-H), 8.20 (d, 1H, $J = 8.0$ Hz, Ar-H), 8.26 (d, 1H, $J = 7.5$ Hz, Ar-H), 8.72 (s, 1H, N = CH), 12.58 (s, 1H, NH). ^{13}C NMR: 122.8, 123.9, 125.5, 126.2, 126.5, 125.6, 126.9, 126.9, 127.1, 127.1, 127.7, 127.8, 128.7, 128.8, 139.1, 150.0, 157.7. MS (m/z , %): (M^+ 357.19, 14.32), ($\text{M}^+ + 1$ 358.26, 5.77), 360.32 (100.00). Analysis calculated for $\text{C}_{21}\text{H}_{15}\text{N}_3\text{O}_2\text{S}$: C, 70.57; H, 4.23; N, 11.76.

41: Greenish white crystals, yield %: 90.3, m.p.: 333–335 °C. ^1H NMR (DMSO- d_6): δ 7.29–7.38 (m, 4H, Ar-H), 7.77–7.80 (m, 2H, Ar-H), 7.93–7.97 (m, 2H, Ar-H), 8.72 (s, 1H, N = CH), 12.39 (s, 1H, NH). ^{13}C NMR: 115.9, 116.1, 129.7, 130.4, 130.7, 143.8, 150.0, 156.2, 160.5, 162.4, 162.9, 164.4, 164.9. MS (m/z , %): (M^+ 299.32, 0.80), 165.10 (100.00). Analysis calculated for $\text{C}_{15}\text{H}_{10}\text{FN}_3\text{O}_2\text{S}$: C, 60.19; H, 3.37; N, 14.04.

4.1.8. Synthesis of N'-(4-substituted benzoyl)benzo[d]thiazole-2-carbohydrazides (44 and 45)

To a solution of benzothiazole-2-carbohydrazide (**33**, 0.193 g, 0.001 mol) in glacial acetic acid (10 ml), the appropriate benzoyl chloride (**42** or **43**, 0.001 mol) was added dropwise and the reaction mixture was stirred at room temperature for about 10 min. The precipitate formed was filtered, washed with water and recrystallized from ethanol.

44: White crystals, yield %: 87, m.p.: 203–205 °C (reported m.p. 191 °C) [21]. ^1H NMR (DMSO- d_6): δ 7.46–7.58 (m, 6H, Ar-H), 7.99 (d, 1H, $J = 7.5$ Hz, Ar-H), 8.17 (d, 1H, $J = 8.5$ Hz, Ar-H), 8.74 (s, 1H, NH), 9.95 (s, 1H, NH).

45: White crystals, yield %: 92, m.p.: 290–292 °C. ^1H NMR (DMSO- d_6): δ 7.34–7.39 (m, 2H, Ar-H), 7.60–7.68 (m, 2H, Ar-H), 7.93–8.00 (m, 2H, Ar-H), 8.19 (d, 1H, $J = 7.5$ Hz, Ar-H), 8.27 (d, 1H, $J = 7.5$ Hz, Ar-H), 10.56 (s, 1H, NH), 10.72 (s, 1H, NH). ^{13}C NMR: δ 115.6, 123.1, 124.2, 127.3, 128.7, 130.2, 135.9, 152.7, 158.6, 159.1, 162.6, 163.3, 164.1. MS (m/z , %): (M^+ 315.46, 28.99), 155.42 (100.00). Analysis calculated for $\text{C}_{15}\text{H}_{10}\text{FN}_3\text{O}_2\text{S}$: C, 57.14; H, 3.20; N, 13.33.

4.1.9. Synthesis of 2-(benzo[d]thiazole-2-carbonyl)-N-(p-substituted phenyl)hydrazine-1-carbothioamides (50–53)

To a solution of benzothiazole-2-carbohydrazide (**33**, 0.193 g, 0.001 mol) in glacial acetic acid (10 ml), the appropriate phenyl isothiocyanate (**46–49**, 0.001 mol) was added dropwise and the reaction mixture was stirred at room temperature for 1–3 h. The precipitate formed was filtered, washed with water and recrystallized from ethanol.

50: White crystals, yield %: 84, m.p.: 170–171 °C. ^1H NMR (DMSO- d_6): δ 2.26 (s, 3H, CH_3), 7.11 (d, 2H, $J = 8.0$ Hz, Ar-H), 7.31 (d, 2H, $J = 8.0$ Hz, Ar-H), 7.58–7.66 (m, 2H, Ar-H), 8.16 (d, 1H, $J = 8.5$ Hz, Ar-H), 8.25 (d, 1H, $J = 7.5$ Hz, Ar-H), 9.77 (s, 1H, NH), 9.82 (s, 1H, NH), 11.16 (s, 1H, NH). ^{13}C NMR: δ 20.6, 116.8, 123.0, 124.1, 125.8, 127.1, 127.2, 128.5, 130.3, 135.9, 136.8, 137.9, 152.7, 163.1. MS (m/z , %): (M^+ 342.27, 40.83), ($\text{M}^+ + 1$ 343.27, 26.14), 206.44 (100.00). Analysis calculated for $\text{C}_{16}\text{H}_{12}\text{N}_4\text{S}_2$: C, 59.24; H, 3.73; N, 17.27.

51: White crystals, yield %: 90, m.p.: 190–192 °C (reported m.p. 196 °C) [22]. ^1H NMR (DMSO- d_6): δ 7.36–7.39 (m, 4H, Ar-H), 7.59–7.66 (m, 2H, Ar-H), 8.16 (d, 1H, $J = 8.5$ Hz, Ar-H), 8.26 (d, 1H, $J = 7.5$ Hz, Ar-H), 9.92 (s, 1H, NH), 9.99 (s, 1H, NH), 11.21 (s, 1H, NH), 10.86 (s, 1H, NH).

52: White crystals, yield %: 86, m.p.: 170–172 °C (reported m.p. 168 °C) [22]. ^1H NMR (DMSO- d_6): δ 3.73 (s, 3H, OCH_3), 6.87–6.90 (m, 2H, Ar-H), 7.27 (d, 2H, $J = 7.5$ Hz, Ar-H), 7.58–7.65 (m, 2H, Ar-H), 8.15 (d, 1H, $J = 7.5$ Hz, Ar-H), 8.24 (d, 1H, $J = 7.5$ Hz, Ar-H), 9.41 (br s, 1H, NH), 9.72 (s, 1H, NH), 10.81 (s, 1H, NH).

53: White crystals, yield %: 88, m.p.: 178–180 °C. ^1H NMR

(DMSO- d_6): δ 6.95–6.99 (m, 4H, Ar-H), 7.10–7.14 (m, 1H, Ar-H), 7.36–7.39 (m, 4H, Ar-H), 7.58–7.66 (m, 2H, Ar-H), 8.16 (d, 1H, $J = 8.0$ Hz, Ar-H), 8.25 (d, 1H, $J = 7.5$ Hz, Ar-H), 9.84 (s, 1H, NH), 9.89 (s, 1H, NH), 11.19 (s, 1H, NH). ^{13}C NMR: δ 118.1, 118.4, 118.7, 123.0, 123.3, 124.1, 127.1, 127.3, 130.0, 134.4, 134.6, 135.9, 152.7, 153.7, 156.8, 162.9, 180.6. MS (m/z , %): (M^+ 420.65, 31.21), 114.17 (100.00). Analysis calculated for $\text{C}_{21}\text{H}_{16}\text{N}_4\text{O}_2\text{S}_2$: C, 59.98; H, 3.84; N, 13.32.

4.1.10. Synthesis of 5-(benzo[d]thiazol-2-yl)-4-(*p*-substituted phenyl)-4*H*-1,2,4-triazole-3-thiols (54–57)

A mixture of the appropriate thiourea derivative (50–53, 0.001 mol) in 40 ml 2 N sodium hydroxide was heated under reflux for 4–24 h, then the reaction mixture was poured into acidic water. The separated product was filtered, dried and recrystallized from ethanol.

54: White crystals, yield %: 63, m.p.: 188–190 °C. ^1H NMR (CDCl_3): δ 2.49 (s, 3H, CH_3), 7.31 (d, 2H, $J = 8.0$ Hz, Ar-H), 7.37 (d, 2H, $J = 8.5$ Hz, Ar-H), 7.42–7.48 (m, 2H, Ar-H), 7.86 (d, 1H, $J = 8.0$ Hz, Ar-H), 7.91 (d, 1H, $J = 8.0$ Hz, Ar-H), 11.72 (s, 1H, SH). ^{13}C NMR: δ 21.4, 121.5, 124.5, 126.7, 126.9, 128.2, 130.2, 130.9, 134.8, 140.5, 146.4, 151.8, 152.8. MS (m/z , %): (M^+ 324.28, 100.00), ($M^+ + 1$ 325.17, 45.34). Analysis calculated for $\text{C}_{16}\text{H}_{12}\text{N}_4\text{S}_2$: C, 59.24; H, 3.73; N, 17.27.

55: White crystals, yield %: 31, m.p.: 273 °C (reported m.p. 268 °C) [22]. ^1H NMR (CDCl_3): δ 7.41 (d, 2H, $J = 9.0$ Hz, Ar-H), 7.49–7.52 (m, 2H, Ar-H), 7.56–7.57 (m, 2H, Ar-H), 7.99 (d, 1H, $J = 8.0$ Hz, Ar-H), 8.18 (d, 1H, $J = 8.0$ Hz, Ar-H).

56: White crystals, yield %: 53, m.p.: 218–220 °C (reported m.p. 242 °C) [22]. ^1H NMR (CDCl_3): δ 3.91 (s, 3H, OCH_3), 7.07 (d, 2H, $J = 9.0$ Hz, Ar-H), 7.34 (d, 2H, $J = 9.0$ Hz, Ar-H), 7.42–7.49 (m, 2H, Ar-H), 7.86 (d, 1H, $J = 7.5$ Hz, Ar-H), 7.92 (d, 1H, $J = 7.5$ Hz, Ar-H), 11.68 (s, 1H, SH).

57: White crystals, yield %: 41, m.p.: 128–130 °C. ^1H NMR (CDCl_3): δ 7.01–7.12 (m, 6H, Ar-H), 7.33–7.36 (m, 2H, Ar-H), 7.52–7.62 (m, 2H, Ar-H), 7.74 (d, 1H, $J = 8.5$ Hz, Ar-H), 8.01 (d, 1H, $J = 7.5$ Hz, Ar-H), 8.13 (d, 1H, $J = 8.5$ Hz, Ar-H), 9.31 (s, 1H, SH). ^{13}C NMR: δ 118.4, 118.6, 119.6, 120.0, 121.4, 121.9, 122.5, 123.2, 123.2, 124.2, 127.0, 129.7, 132.3, 134.9, 137.3, 150.8, 160.5. MS (m/z , %): (M^+ 402.06, 34.93), 76.24 (100.00). Analysis calculated for $\text{C}_{21}\text{H}_{14}\text{N}_4\text{OS}_2$: C, 62.67; H, 3.51; N, 13.92.

4.1.11. Synthesis of *N'*-(benzo[d]thiazole-2-carbonyl)-*p*-substituted benzenesulfonohydrazides (60 and 61)

To a solution of benzothiazole-2-carbohydrazide (33, 0.193 g, 0.001 mol) in glacial acetic acid (10 ml), the appropriate benzenesulfonyl chloride (58 or 59, 0.001 mol) was added and the reaction mixture was stirred at room temperature for 1–3 h. The precipitate formed was filtered, washed with water and recrystallized from ethanol.

60: White crystals, yield %: 84, m.p.: 283–285 °C. ^1H NMR (CDCl_3): δ 7.50–7.57 (m, 2H, Ar-H), 7.62 (d, 2H, $J = 7.0$ Hz, Ar-H), 7.75 (s, 1H, NH), 7.81 (d, 2H, $J = 7.0$ Hz, Ar-H), 7.97 (d, 1H, $J = 8.5$ Hz, Ar-H), 8.12 (d, 1H, $J = 8.0$ Hz, Ar-H), 9.23 (s, 1H, NH). ^{13}C NMR: δ 122.3, 124.8, 127.4, 127.6, 129.5, 129.9, 132.4, 135.3, 136.8, 152.5, 158.3, 158.9. MS (m/z , %): (M^+ 412.14, 25.86), 178.25 (100.00). Analysis calculated for $\text{C}_{14}\text{H}_{10}\text{BrN}_3\text{O}_3\text{S}_2$: C, 40.79; H, 2.44; N, 10.19.

61: White crystals, yield %: 78, m.p.: 200–203 °C. ^1H NMR (DMSO- d_6): δ 2.37 (s, 3H, CH_3), 7.35 (d, 2H, $J = 7.5$ Hz, Ar-H), 7.57–7.65 (m, 2H, Ar-H), 7.71 (d, 2H, $J = 8.5$ Hz, Ar-H), 8.13 (d, 1H, $J = 8.0$ Hz, Ar-H), 8.21 (d, 1H, $J = 7.5$ Hz, Ar-H), 10.18 (s, 1H, NH), 11.30 (s, 1H, NH). ^{13}C NMR: δ 21.0, 123.0, 124.2, 127.2, 127.3, 127.6, 129.4, 135.8, 136.3, 143.3, 152.6, 159.0, 162.0. MS (m/z , %): (M^+ 347.97, 6.89), ($M^+ + 1$ 348.88, 1.54), 91.08 (100.00). Analysis calculated for $\text{C}_{15}\text{H}_{13}\text{N}_3\text{O}_3\text{S}_2$: C, 51.86; H, 3.77; N, 12.10.

4.2. Biological evaluation

4.2.1. Cytotoxicity assay

Cell lines were cultured in RPMI-1640 medium with 10% fetal bovine serum. Antibiotics added were 100 units/ml penicillin and 100 $\mu\text{g}/\text{ml}$ streptomycin at 37 °C in a 5% CO_2 incubator. The cell lines were seeded in a 96-well plate at a density of 1.0×10^4 cells/well at 37 °C for 48 h under 5% CO_2 . After incubation, the cells were treated with different concentrations of compounds and incubated for 24 h. After 24 h of drug treatment, 20 μl of MTT solution at 5 mg/ml were added and incubated for 4 h. Dimethyl sulfoxide (DMSO) in volume of 100 μl was added into each well to dissolve the purple formazan formed. The colorimetric assay was measured and recorded at absorbance of 570 nm using a plate reader (EXL 800, USA). The relative cell viability in percentage was calculated as (A_{570} of treated samples/ A_{570} of untreated sample) $\times 100$ [10,11].

4.2.2. EGFR inhibitory activity

Lapatinib as an EGFR inhibitor was used as a positive control, in addition to DMSO was used as a negative control, and the test compounds were pre-incubated with EGFR kinase for 10 to 30 min prior to adding ATP/substrate in order to initiate kinase reaction in 96-well plate. 5 μl of ATP and kinase substrate were then added to each well and left to be incubated for 30 min. Fluorimetric assay method was used to quantify the ADP produced as a result of kinase reaction. Intensity of fluorescence decreased as the strength of the test compound inhibitory activity increased [12,13].

4.3. Molecular modeling studies

Three-dimensional structures of selected synthesized active EFGR inhibitors in their neutral forms were drawn using the MOE of Chemical Computing Group Inc software. Conformational analysis study was performed where the lowest energy conformer ‘global-minimum’ was identified for each derivative. The following step was docking of the best conformer into the EFGR enzyme-binding domain. The 1xkk pdb crystal structure of EFGR enzyme was chosen for docking, it was co-crystallized with lapatinib ligand, a potent EFGR inhibitor [14] which was used as a reference in our docking study. For the preparation of docking process, the co-crystallized ligand was removed and the enzyme was 3D protonated. Hydrogen atoms were added at their standard geometry, the partial charges were conducted then energy optimization was computed. Docking was run using triangle matcher as placement method and affinity dG as a scoring function. 30 conformers of the ligand were retained with the highest and best score. To validate the docking procedure and results, lapatinib was docked into the active site ligand receptor interaction *via* docking which was demonstrated by 2D and 3D ligand views. The active site has been defined as the collection of residues with the bound inhibitor and comprised the union of all ligands of the ensemble. All atoms located $< 10.0 \text{ \AA}$ from any ligand atom were considered. The investigated compounds were subjected to surface mapping and alignment experiments [23–27] using ‘Molecular Operating Environment’ software (MOE of Chemical Computing Group Inc., on a Core i7 workstation).

Declaration of Competing Interest

The authors declare that they have no known competing financial interests or personal relationships that could have appeared to influence the work reported in this paper.

Appendix A. Supplementary material

Supplementary data to this article can be found online at <https://doi.org/10.1016/j.bioorg.2020.104259>.

References

- [1] D. Hanahan, R.A. Weinberg, The hallmarks of cancer, *Cell* 100 (2000) 57–70.
- [2] R.S. Herbst, Review of epidermal growth factor receptor biology, *Int. J. Radiat. Oncol. Biol. Phys.* 59 (2004) 21–26.
- [3] H. Zhang, A. Berezov, Q. Wang, G. Zhang, J. Drebin, R. Murali, M.I. Greene, ErbB receptors: from oncogenes to targeted cancer treatment, *J. Clin. Invest.* 117 (2007) 2051–2058.
- [4] A. Petrelli, S. Giordano, From single- to multi-target drugs in cancer therapy: When aspecificity becomes an advantage, *Curr. Med. Chem.* 15 (2008) 422–432.
- [5] W. Pao, V. Miller, M. Zakowski, J. Doherty, K. Politi, I. Sarkaria, B. Singh, R. Heelan, V. Rusch, L. Fulton, E. Mardis, D. Kupfer, R. Wilson, M. Kris, H. Varmus, EGF receptor gene mutations are common in lung cancers from 'never smokers' and are associated with sensitivity of tumors to gefitinib and erlotinib, *Proc. Natl. Acad. Sci. USA* 101 (2004) 13306–13311.
- [6] H.W. Lo, S.C. Hsu, M.C. Hung, EGFR signaling pathway in breast cancers: From traditional signal transduction to direct nuclear translocalization, *Breast Cancer Res. Treat.* 95 (2006) 211–218.
- [7] S. Tasler, O. Muller, T. Wieber, T. Herz, R. Krauss, F. Totzke, M.H.G. Kubbutat, C. Schachtele, *N*-substituted 2'-(aminoaryl)benzothiazoles as kinase inhibitors: Hit identification and scaffold hopping, *Bioorg. Med. Chem. Lett.* 19 (2009) 1349–1356.
- [8] M.T. Gabr, N.S. El-Gohary, E.R. El-Bendary, M.M. El-Kerdawy, EGFR tyrosine kinase targeted compounds: *in vitro* antitumor activity and molecular modeling studies of new benzothiazole and pyrimido[2,1-*b*]benzothiazole derivatives, *EXCLI J.* 13 (2014) 573–585.
- [9] M. Singh, S.K. Singh, B. Thakur, P. Ray, S.K. Singh, Design and synthesis of novel Schiff base-benzothiazole hybrids as potential epithelial growth factor receptor (EGFR) inhibitors, *Anti-Cancer Agents Med. Chem.* 16 (2016) 722–739.
- [10] T. Mosmann, Rapid colorimetric assay for cellular growth and survival: application to proliferation and cytotoxicity assays, *J. Immunol. Methods* 65 (1983) 55–63.
- [11] F. Denizot, R. Lang, Rapid colorimetric assay for cellular growth and survival: modifications to the tetrazolium dye procedure giving improved sensitivity and reliability, *J. Immunol. Methods* 89 (1986) 271–277.
- [12] G. Manning, D.B. Whyte, R. Martinez, T. Hunter, S. Sudarsanam, The protein kinase complement of the human genome, *Science* 298 (2002) 1912–1934.
- [13] S.K. Grant, Therapeutic protein kinase inhibitors, *Cell. Mol. Life Sci.* 66 (2009) 1163–1177.
- [14] E.R. Wood, A.T. Truesdale, O.B. McDonald, D. Yuan, A. Hassell, S.H. Dickerson, B. Ellis, C. Pennisi, E. Horne, K. Lackey, K.J. Alligood, D.W. Rusnak, T.M. Gilmer, L. Shewchuk, A unique structure for epidermal growth factor receptor bound to GW572016 (Lapatinib): relationships among protein conformation, inhibitor off-rate, and receptor activity in tumor cells, *Cancer Res.* 64 (2004) 6652–6659.
- [15] H. Behbehani, H.M. Ibrahim, 4-Thiazolidinones in heterocyclic synthesis: synthesis of novel enamines, azolopyrimidines and 2-arylimino-5-arylidene-4-thiazolidinones, *Molecules* 17 (2012) 6362–6385.
- [16] O.A. Saleh, M.F. El-Behery, M.N. Aboul-Enein, A.A. El-Azzouny, Y.A. Maklad, Anticonvulsant potential of certain *N*-(6-substituted benzo[*d*]thiazol-2-yl)-2-(4-substituted piperazin-1-yl)acetamides, *Egypt. Pharmaceut. J.* 15 (2016) 62–69.
- [17] A. Kumar, A.K. Shakya, H.H. Siddiqui, Synthesis and anti-inflammatory activity of some novel 2-aminobenzothiazole derivatives, *Ind. J. Het. Chem.* 25 (2016) 243–249.
- [18] U.D. Ozkay, O.D. Can, Y. Ozkay, Y. Ozturk, Effect of benzothiazole/piperazine derivatives on intracerebro ventricular streptozotocin-induced cognitive deficits, *Pharmacol. Rep.* 64 (2012) 834–847.
- [19] D. Havrylyuk, L. Mosula, B. Zimenkovsky, O. Vasylenko, A. Gzella, R. Lesyk, Synthesis and anticancer activity of 4-thiazolidinones containing benzothiazole moiety, *Eur. J. Med. Chem.* 45 (2010) 5012–5021.
- [20] B. Rajeeva, N. Srinivasulu, S.M. Shantakumar, Synthesis and antimicrobial activity of some new 2-substituted benzothiazole derivatives, *E.-J. Chem.* 6 (2009) 775–779.
- [21] S.N. Sawhney, S. Janvijay, O.P. Bansal, Benzothiazole derivatives. IV. Synthesis of some 2- and 6-(1,3,4-oxadiazol-2-yl)benzothiazoles and 2- and 6-(1,3,4-thiadiazol-2-yl)benzothiazole as potential anti-inflammatory agents, *Ind. J. Chem. Soc.* 51 (1974) 886–890.
- [22] S.N. Sawhney, S. Janvijay, O.P. Bansal, Benzothiazole derivatives. V. Synthesis of some 2-(5'-substituted amino-1',3',4'-oxadiazol-2'-yl), 2-(5'-substituted amino-1',3',4'-thiadiazol-2'-yl) and 2-(3'-mercapto-4'-substituted 4*H*-1',2',4'-triazol-5'-yl) benzothiazole as potential anti-inflammatory agents, *Ind. J. Chem. Soc.* 13 (1975) 804–807.
- [23] P. Labute, C. Williams, M. Feher, E. Sourial, J.M. Schmidt, Flexible alignment of small molecules, *J. Med. Chem.* 44 (2001) 1483–1490.
- [24] V. Cody, C.H. Schwalbe, Structural characteristics of antifolate dihydrofolate reductase enzyme interactions, *Crystallogr. Rev.* 12 (2006) 301–333.
- [25] J.P. Volpato, B.J. Yachnin, J. Blanchet, V. Guerrero, L. Poulin, E. Fossati, A.M. Berghuis, J.N. Pelletier, Multiple conformers in active site of human dihydrofolate reductase F31R/Q35E double mutant suggest structural basis for methotrexate resistance, *J. Biol. Chem.* 284 (2009) 20079–20089.
- [26] N. L. Allinger, Conformational analysis. 130. MM2. A hydrocarbon force field utilizing V1 and V2 torsional terms, *J. Am. Chem. Soc.* 99 (1977) 8127–8134.
- [27] S.K. Kearsley, G.M. Smith, An alternative method for the alignment of molecular structures: Maximizing electrostatic and steric overlap, *Tetrahedron Comput. Methodol.* 3 (1990) 615–633.